AGU PUBLICATIONS

Geophysical Research Letters

RESEARCH LETTER
10.1002/2017GL075255

Key Points:
- We seismically image Yellowstone's iconic hydrothermal system utilizing stationary hydrothermal activity as a seismic source
- We constrain how shallow geologic structure and fluid pathways control the formation and location of Old Faithful geyser and the Upper Geyser Basin hydrothermal system
- We image a relatively large and shallow, 10-60 m, 200 m wide hydrothermal reservoir centered ~100 m southwest of Old Faithful geyser

Supporting Information:
- Supporting Information S1
- Figure S1
- Figure S2
- Movie S1

Correspondence to:
S.-M. Wu,
sinmei.wu@utah.edu

Citation:
Wu, S.-M., Ward, K. M., Farrell, J., Lin, F.-C., Karplus, M., & Smith, R. B. (2017). Anatomy of Old Faithful from subsurface seismic imaging of the Yellowstone Upper Geyser Basin. *Geophysical Research Letters*, *44*. https://doi.org/10.1002/2017GL075255

Received 9 AUG 2017
Accepted 28 SEP 2017
Accepted article online 3 OCT 2017

Anatomy of Old Faithful From Subsurface Seismic Imaging of the Yellowstone Upper Geyser Basin

Sin-Mei Wu[1], Kevin M. Ward[1], Jamie Farrell[1], Fan-Chi Lin[1], Marianne Karplus[2], and Robert B. Smith[1]

[1]Department of Geology and Geophysics, University of Utah, Salt Lake City, UT, USA, [2]Department of Geological Sciences, University of Texas at El Paso, El Paso, TX, USA

Abstract The Upper Geyser Basin in Yellowstone National Park contains one of the highest concentrations of hydrothermal features on Earth including the iconic Old Faithful geyser. Although this system has been the focus of many geological, geochemical, and geophysical studies for decades, the shallow (<200 m) subsurface structure remains poorly characterized. To investigate the detailed subsurface geologic structure including the hydrothermal plumbing of the Upper Geyser Basin, we deployed an array of densely spaced three-component nodal seismographs in November of 2015. In this study, we extract Rayleigh wave seismic signals between 1 and 10 Hz utilizing nondiffusive seismic waves excited by nearby active hydrothermal features with the following results: (1) imaging the shallow subsurface structure by utilizing stationary hydrothermal activity as a seismic source, (2) characterizing how local geologic conditions control the formation and location of the Old Faithful hydrothermal system, and (3) resolving a relatively shallow (10–60 m) and large reservoir located ~100 m southwest of Old Faithful geyser.

1. Introduction

Yellowstone National Park contains the largest concentration of hydrothermal features with over 10,000 geysers, hot springs, fumaroles, etc. (Smith & Siegel, 2000). Most of the hydrothermal features are located within or on the margins of the 0.63 Ma and youngest Yellowstone caldera where the hydrothermal system has been shown to be driven by the interaction between a deeper mantle-crust magmatic system and the shallow hydrologic system (Christiansen et al., 2007; Smith et al., 2009; Waite et al., 2006). The Upper Geyser Basin (UGB), which hosts Old Faithful geyser and many other active hydrothermal features, is located on the western edge of the Mallard Lake resurgent dome and is located in the Firehole River valley in between the 0.124 Ma and 0.164 Ma postcaldera rhyolite flows. The hydrothermal systems within Yellowstone have been the subject of many geophysical, geochemical, and biological investigations to understand this unperturbed hydrothermal system including a summary by Hurwitz and Lowenstern (2014).

Knowledge of the subsurface in the UGB is known mostly from scientific drilling. In 1929, the Carnegie Institute drilled hole C-1 in the Myriad Group (Figure 1a) (Fenner, 1936), and in 1967, the U.S. Geological Survey drilled three holes in Black Sand Basin and Biscuit Basin (White et al., 1975). Results from well C-1 suggest a ~65 m thick glacial gravel layer overlaying hydrothermally altered rhyolite. While the surface geology in the area can be roughly separated into ~20 m wide mounds of rhyolitic lava deposits on the northeast, glacial deposits on the southwest, and hydrothermal deposits covering a significant portion of the UGB (Abendini et al., 2015; Christiansen, 2001; Fenner, 1936; Muffler et al., 1982), the subsurface lateral structure variations which likely control the subsurface plumbing and fluid migration properties are not well constrained.

Located within the UGB, Old Faithful geyser is arguably the most famous geyser in the world and has been studied using different geophysical measurements trying to understand its periodic eruption mechanism. In a series of in situ experiments from 1983 to 1993, pressure and temperature probes and a special ice-cooled video camera were lowered into Old Faithful geyser providing an image and geometry of the geyser conduit to ~22 m depth (Hutchinson et al., 1997; https://www.youtube.com/watch?v=8luNCFUnvBw). Several temporary seismic array deployments (including a 96 station dense single-component geophone array) were conducted near Old Faithful that revealed a ~45 min preeruption, harmonic seismic tremor (Kedar et al., 1996, 1998; Kieffer, 1984) prior to geyser eruptions. Persistent seismic tremor associated with bubble collapse within the hydrothermal conduit was observed (Kedar et al., 1996, 1998), and the tremor source locations,

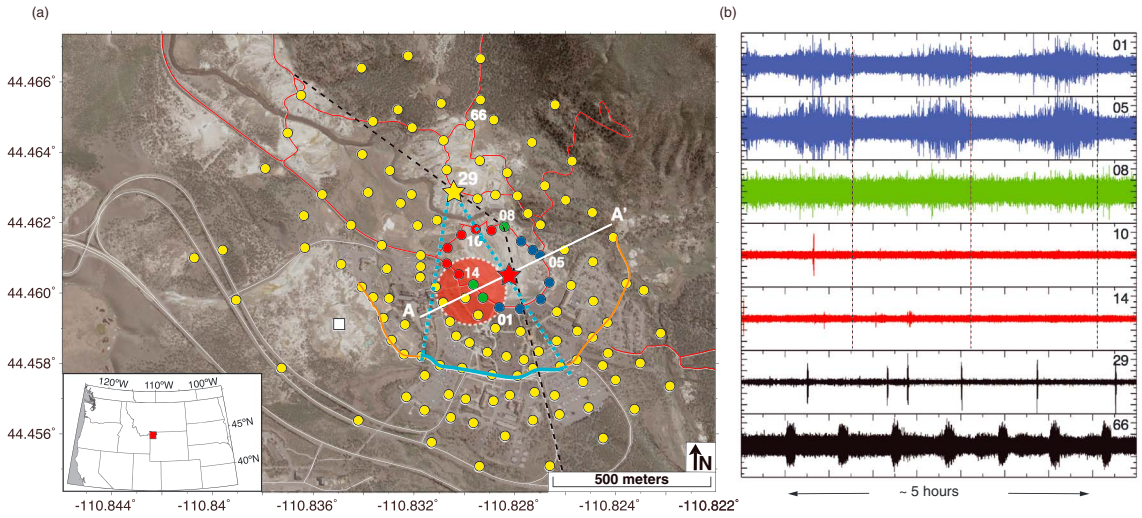

Figure 1. (a) Map of the 2015 Yellowstone Upper Geyser Basin seismic array. The red star marks the location of Old Faithful geyser. Color-coded circles represent the 133 geophone station locations. Gray and red lines mark roads and trails, respectively. The station 029 (yellow star) is considered as the virtual source for noise cross-correlations in this study. The orange and light blue lines denote the receiver stations shown in Figure 3. The dashed black lines delineate the observed seismic velocity boundary. The red circle with dashed white edge illustrates the location of our imaged highly fractured and porous medium for Old Faithful geyser hydrothermal reservoir projected onto the surface. The white line (A-A′) shows the cross section of our schematic model (Figure 4). The white square marks the location of drill hole C-1 (Fenner, 1936). (b) Examples of the seismic signals over 10 Hz from distinct hydrothermal activities. The blue, green, and red color records, corresponding to the stations by the inner boardwalk in Figure 1a, represent the Old Faithful tremor signals can be clearly observed (blue), subtly observed (green), and wholly absent (red). The vertical dashed lines mark Old Faithful geyser eruption time from Geyser Times (http://www.geysertimes.org). The seismic records at station 29 and 66 show distinguished tremor signals that are associated with their nearby hydrothermal features.

derived from beam-forming analysis, were used to infer the presence of a subsurface cavity and recharging dynamics (Vandemeulebrouck et al., 2013). The statistical analysis of geyser eruption intervals was applied to characterize the fluid dynamics and thermodynamics of Old Faithful geyser by comparing the perturbations of the periodicity with the extrinsic variations (e.g., stress, pressure, and temperature) (Hurwitz et al., 2008, 2014). In addition, a mechanical model based on an offset bubble trap was used to simulate the water column resonant frequency within the Old Faithful conduit (Rudolph & Sohn, 2017).

Detailed knowledge of the subsurface structure and geyser fluid are important to understand the hydrothermal fluid migration and geyser eruption mechanism (Hurwitz & Manga, 2017; Hurwitz et al., 2014; Husen et al., 2004; Karlstrom et al., 2013; Marler & White, 1975; Munoz-Saez et al., 2015; Rudolph & Sohn, 2017; Vandemeulebrouck et al., 2013). However, the 3-D subsurface structure of the UGB/Old Faithful hydrothermal system remain largely unconstrained because of the sensitive environmental setting of the Upper Geyser Basin which prevented the implementation of active source seismic imaging around the geyser.

In this study, we investigate detailed subsurface structure using a large-N (N refers to the number of nodes or seismographs) temporary geophone array and passive ambient noise seismic interferometry (e.g., Lin et al., 2013; Wang et al., 2017). Contrary to common noise cross-correlation methods based on a diffusive noise environment, we extract propagating seismic wavefields utilizing the nondiffusive hydrothermal signals excited by nearby stationary hydrothermal activity. While further studies are needed to fully understand the sources of these hydrothermal signals, they are likely related to not only the bubble collapsing events (Kedar et al., 1996, 1998; Kieffer, 1984), which primarily excite hydrothermal tremors at frequencies higher than 10 Hz, but also rapid migration of high-pressure water and steam-filled pathways. At low frequencies (0.5 to 5 Hz), we observed a clear lateral velocity boundary that delineates the higher velocity rhyolitic lava flows on the northeast Mallard Lake resurgent dome from the lower velocity Quaternary glacial deposits along the Firehole River valley on the southwest. At higher frequencies (5 to 10 Hz), spatially dependent waveform distortions are observed west of Old Faithful geyser likely representing a highly fractured and porous hydrothermal reservoir. Integrating existing geologic information with our shallow subsurface seismic results of Old Faithful geyser region advances our understanding of the fluid flow dynamics between the shallow geologic structure and the hydrothermal plumbing system.

2. Data and Methods

2.1. Seismic Array

To explore shallow hydrothermal structure of Old Faithful geyser and surrounding hydrothermal systems, we apply multicomponent ambient noise cross-correlation (Lin et al., 2008) using a temporary array of seismographs. Our specific array was composed of 133 three-component (3C) autonomous 5 Hz nodal geophones deployed from 2 to 14 November 2015. The average station spacing was ~50 m and the full aperture of the array was around 1 km (Figure 1a).

2.2. Challenges in Active Hydrothermal Area

The intense and dynamic hydrothermal activity of the UGB has a substantial influence on recorded seismic signals across our array (i.e., the periodic and nonperiodic tremor signals from hydrothermal fluid and steam migration at low frequency ($<$10 Hz) and boiling water and bubble collapse at high frequency ($>$10 Hz; Figure 1b). These features add complexity in generating empirical seismic Green's functions between each station pair from traditional ambient noise cross-correlation methods. The traditional method normally relies on correlating diffusive seismic signals, which are excited mostly from semievenly distributed far-field noise sources, and then enhancing the seismic signal-to-noise ratio by retrieving average information (stacking) over a longer time period (Bensen et al., 2007; Snieder, 2004). Instead of diffusive noise wavefield, hydrothermal activity within the array generates a much stronger seismic signal compared to the far-field noise source and prevents us from extracting Green's functions from all station pairs. Despite this limitation, some of our stations (referred to as source stations) are close enough to the persistent and active hydrothermal activity that seismic wave propagation across the entire array can be studied using cross-correlation between these source stations and all other stations.

2.3. Constructing Cross-Correlation Functions

The cross-correlation method we applied is similar to the one described in Lin et al. (2013). To suppress the effects of spatial and temporal variations resulting from the hydrothermal tremor signals, we first divided the 13 days of 100 sample-per-second raw data into 60 s windows. We then performed spectral whitening before calculating the cross-correlation functions (CCFs) between all station pairs for all three components (i.e., vertical and horizontals). To preserve the relative amplitude ratios between components (Lin et al., 2014), we perform frequency whitening by dividing the spectrum of each component based on the averaged spectrum of all three components. All available 60 s nine-component CCFs were normalized by the maximum amplitude of the vertical-vertical CCFs before being stacked into the final CCFs.

Coherent signals with a clear moveout in time are observed in the 0.5–5 Hz band passed vertical-vertical noise CCFs between station 029 on Geyser Hill and all other stations across the array (Figure 2a and Movie S1 in the supporting information). These coherent seismic signals demonstrate a delay in the seismic travel times, that is, positive time lag within the CCFs, suggesting the existence of a persistent noise/tremor source located near station 029. We note that although there are numerous hydrothermal features near station 029, the strong coherent signals observed in the CCFs are generally below 10 Hz frequency, which is different from the $>$10 Hz dominant frequency of the hydrothermal tremor signals related to bubble collapse or boiling water observed in raw seismograms of earlier studies of Kedar et al. (1996). In addition to station 029, we identified a few other source stations where coherent seismic signals can be observed in their associated CCFs. However, the signals observed with source station 029 have the best signal-to-noise ratios and will be the focus of the discussion below. While it would be interesting to better understand the source properties of the noise/tremor sources, it is beyond the scope of this study.

2.4. Rayleigh Wave Phase Velocity

Particle motion analysis of ground motion based on multicomponent CCFs suggests that the observed seismic signals emitted by the source station 029 are dominantly Rayleigh waves (surface waves polarized in the vertical and radial directions) with a ~90° phase shift between vertical and horizontal components (Figure S1). To constrain the subsurface structure, we measured Rayleigh wave phase travel times and velocities by applying standard frequency-time analysis (FTAN; Bensen et al., 2007; Lin et al., 2008) on the positive time lag of the vertical-vertical component CCFs. For each period, we follow the phase-front tracking method described by Lin and Ritzwoller (2011) to correct for the 2π phase shift ambiguity for all measurements. Figure 2b shows

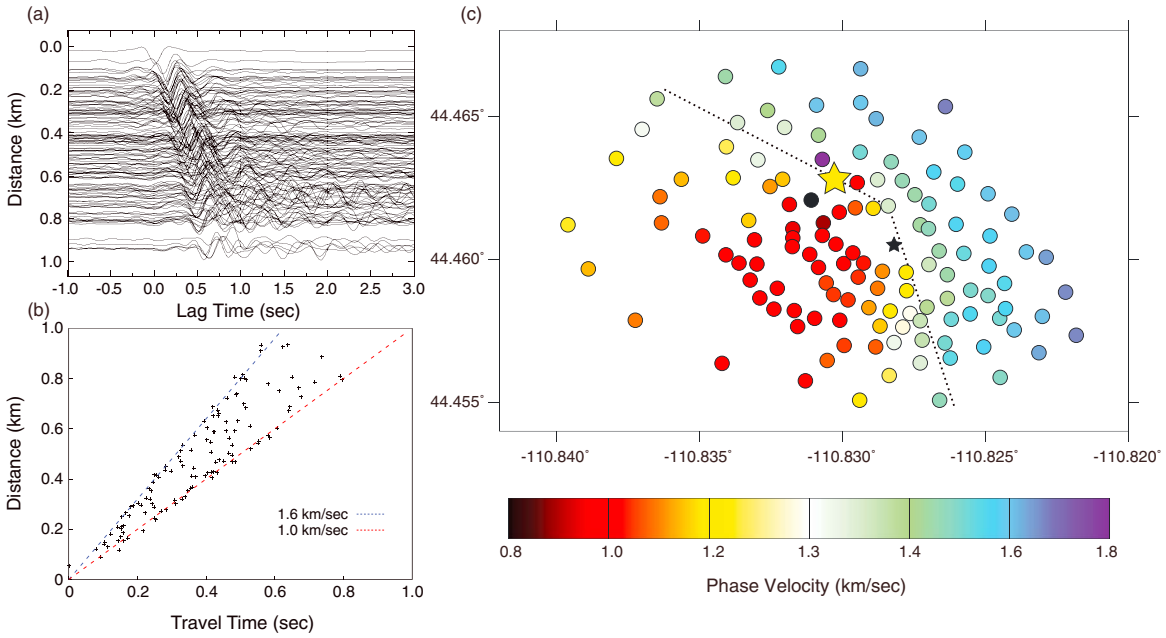

Figure 2. (a) Seismic noise cross-correlation record section (0.5–5 Hz) with station 029 as the common station (zero distance). (b) Phase velocity travel time measurements of Rayleigh waves from vertical-vertical cross-correlation functions between station 029 and all other stations as a function of distance at 3.3 Hz. Two velocity branches can be observed (1.0 and 1.6 km/s). (c) The 3.3 Hz phase velocity measurements between station 029 (yellow star) and all other receiver stations. The dashed black lines delineate the boundary between the fast- and slow-velocity boundary. The black star marks the location of Old Faithful geyser.

the phase travel time and distance relationship at 3.33 Hz between source station 029 and all other stations. Two distinct velocity branches are observed with a fast velocity around 1.6 km/s and a lower velocity around 1.0 km/s suggesting there are two distinct velocity structures in our study area.

3. Results and Discussions

3.1. Seismic Velocity Contrast

The observation of coherent wave propagation across the UGB allows the evaluation of detailed subsurface structural variations across the area. Between 0.5 and 5 Hz, a clear velocity contrast is observed in both CCF waveforms (Figure S2) and Rayleigh wave phase velocity measurements (Figure 2b). Phase velocity measurements at 3.33 Hz shows a ~40% velocity contrast between fast-velocity structure in the northeast and slow-velocity structure in the southwest (Figure 2c). At this frequency, Rayleigh waves are most sensitive to structure in the top 100 m and the striking velocity contrast is likely imaging the compositional difference between the rhyolitic lava in the northeast and glacial deposits in the southwest. We note that the Rayleigh waves propagating across the fast structure in the northeast manifest almost no dispersion (Figure S2), suggesting the subsurface velocity structure is constant over the depths our results have sensitivity (around 10 to 100 m depth). Forward modeling of a half-space layer that fits the phase velocity observations results in a V_s (shear velocity) of ~1.72 km/sec in the northeast and ~1.08 km/s in the southwest. Comparing to rhyolitic lava, the glacial deposits in the southwest are more brittle and fractured, providing fluid pathways to hydrothermal features. Therefore, the existence of the lateral structure boundary might preferentially direct and focus vertically migrating fluid pathways to the southwest Old Faithful geyser area.

3.2. Highly Fractured and Porous Hydrothermal Reservoir

While the observed seismic signals between 0.5 and 5 Hz frequency are relatively coherent and reveal larger-scale subsurface structures, significant waveform variation and distortion are also observed at higher frequencies between 5 and 10 Hz. Figure 3a shows the CCF waveforms excited by source station 029 and observed across a transect of stations on the southeastern side of Old Faithful (see Figure 1a). Clear waveform complexity, group energy delay, and strong coda at high frequencies are observed for waves propagating

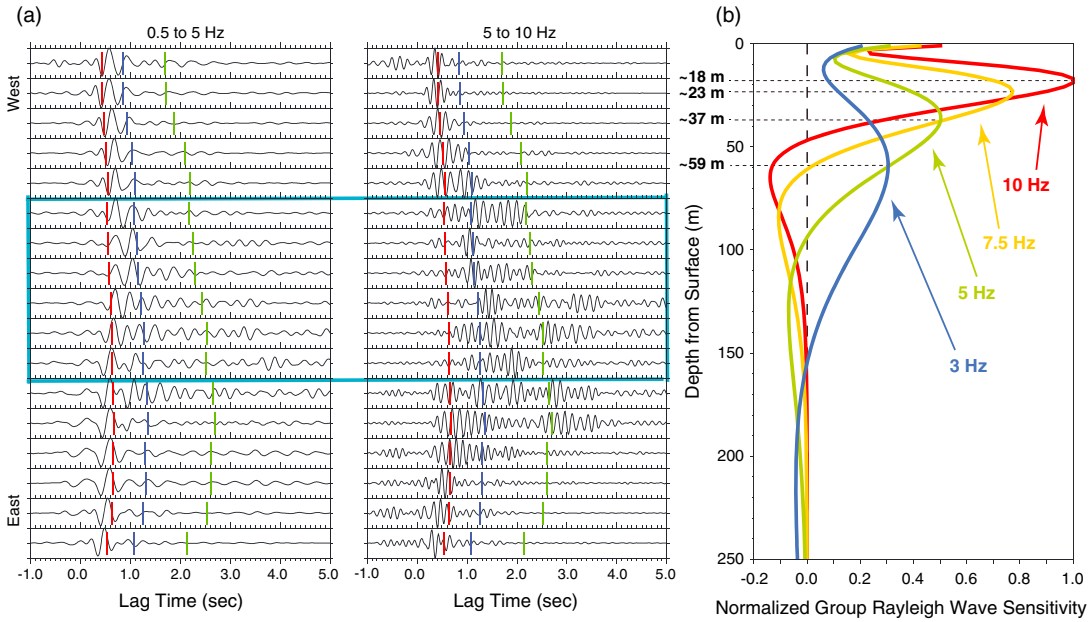

Figure 3. (a) Seismic noise vertical-vertical cross-correlations for 0.5–5 Hz (left panel), and 5–10 Hz (right panel) between 029 and receiver stations located on the orange and light blue lines shown in Figure 1. The red, blue, and green bars show the predicted travel time by assuming the seismic velocities at 1.0, 0.5, and 0.25 km/s, respectively. The waveforms within the light blue box correspond to the receiver stations located on the light blue lines in Figure 1. (b) Rayleigh wave group velocity sensitivity kernels at 3, 5, 7.5, and 10 Hz based on a uniform 1.078 km/s V_s 1-D half-space model.

through the immediate western side of the Old Faithful cone. This suggests the presence of a highly localized, strongly heterogeneous and shallow, low-velocity anomaly adjacent to Old Faithful geyser. The more impulsive waveforms observed on both the eastern and western sections of our dense transect constrain the longitudinal dimension of the anomaly. Note that while the eastern side of the waveform transition is near the structural boundary observed in the lower frequencies (Figure 2c), a similar transition/boundary does not exist on the western side. We interpret this shallow and rather confined slow-velocity anomaly as a localized, highly fractured, and porous body within the glacial deposit.

The presence of a highly fractured and porous medium is manifest in the observations of spatial-dependent hydrothermal tremor signals recorded by stations close to Old Faithful geyser. In our array, there are 16 stations located near the closest boardwalk around Old Faithful with a radius of ~120 m. Clear tremor signals excited by bubble collapse from Old Faithful geyser with a periodicity of ~93 min with a dominant frequency range of 10–20 Hz can be observed at stations near the eastern part of the boardwalk. However, there is no corresponding tremor signal observed at stations located near the western part of the boardwalk (Figure 1b). The dramatic difference in seismic wave propagation within a spatial distance of less than 300 m suggests a stronger wave attenuating medium beneath the geyser sinter in the west compared to the east.

3.3. Estimated Dimension and Capacity of the Hydrothermal Reservoir

The subsurface geometries of the plumbing system are unique to different geysers, and how fluid and gasses migrate between these subsurface hydrothermal reservoirs and the surficial geyser expression is key to understanding geyser eruption dynamics. The comparison between the capacity of the reservoir and the actual erupted water volume can also provide an insight into fluid interaction processes between deep and shallow reservoir structures. From the spatial distribution of stations that observe the distorted seismic waves at 5–10 Hz frequency (Figure 3a, right panel), we estimate the horizontal extent of the subsurface highly fractured and porous medium to be around 200 m in diameter. The depth of this hydrothermal reservoir is constrained from Rayleigh wave group velocity sensitivity kernels (Figure 3b) generated from the 1-D half-space 1.08 km/s V_s model. The Rayleigh waves at this frequency (5–10 Hz) are most sensitive to the velocity structure around 10–60 m and constrain the vertical extent of the subsurface reservoir. From the observed cross-correlated waveform distortions between 5 and 10 Hz, we measure the Rayleigh wave

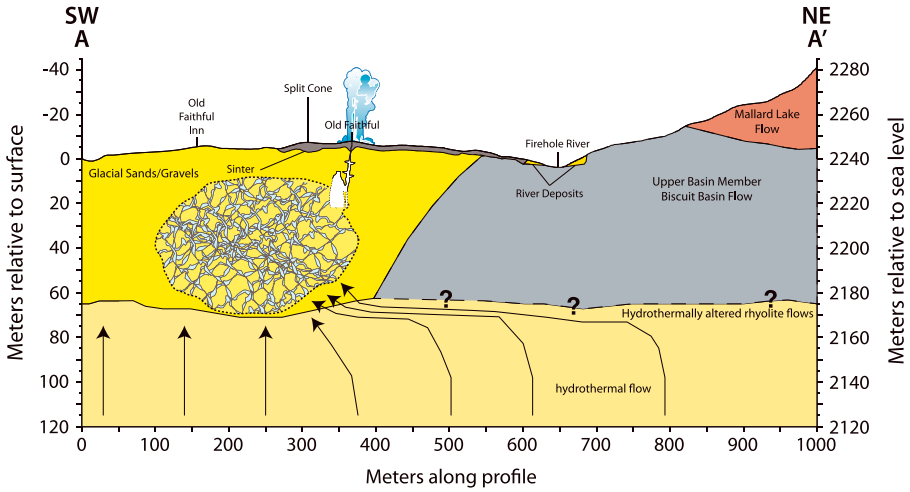

Figure 4. The interpreted of the Old Faithful geyser plumbing system based on the results of this study. Our working model is constrained by nearby geological structure based on geological mapping and previous drilling results (Christiansen, 2001; Fenner, 1936; Muffler et al., 1982; Vandemeulebrouck et al., 2013; White et al., 1975). This cross section follows the AA′ white line in Figure 1. The ascending hydrothermal flow is assumed to be redirected by the impermeable Biscuit Basin flow to the highly fractured and porous medium west of the glacial deposit/rhyolitic lava boundary. Dashed lines with question marks are inferred based upon hydrothermal models and mapped geology.

group velocity at 7.5 Hz from our FTAN analysis. The measured group velocities are ~1.13 km/s within the glacial deposit near the western end of our transect and as low as ~0.33 km/s across our imaged shallow reservoir. This represents a group velocity reduction of ~70%, which we assume results mostly from the porosity contrast across the different deposits. We note that Rayleigh waves are mostly sensitive to shear velocity structure, which is extremely sensitive to the degree of fluid content. With Rayleigh waves alone, however, we cannot distinguish steam from liquid phase, as both phases have zero shear velocity.

We follow the method described by Chu et al. (2010) to model the effects of porosity on shear velocity. Despite the fact that glacial deposits observed at the surface in our study area are different from those modeled in Chu et al. (2010), here our intention is to determine a first-order estimation of the fluid content. Assuming a 70% velocity reduction as observed in our Rayleigh wave group velocity at 7.5 Hz, a porosity around ~30% is needed to explain our imaged subsurface porous medium. Approximating the porous medium is ellipsoidal shaped with a diameter of 200 m and a height of 50 m; the volume of the porous medium is about 1×10^6 m^3. With a porosity of ~30%, we estimate the volume of the reservoir to be around ~300,000 m^3. This estimate is much larger than the estimated 20–40 m^3 per single Old Faithful eruption (Allen & Day, 1935; Kieffer, 1984), consistent with the assumption that only a small portion of the fluid within the entire hydrothermal plumbing system is involved in each eruption (Hurwitz & Manga, 2017). According to an earlier tracer experiment (Fournier, 1969), Old Faithful geyser requires at least 24 eruptions to clear the tracer within its directly connected plumbing system. We suggest that the imaged hydrothermal reservoir likely provides a steady fluid influx to the shallower plumbing system.

3.4. Proposed Model of the Subsurface Hydrothermal System

The proposed bubble trap of Old Faithful geyser system as interpreted by Vandemeulebrouck et al. (2013) was modeled to be located slightly to the west of Old Faithful geyser conduit with the central depth below 15 m and as wide as ~20 m. The hydrothermal reservoir imaged in our study, with a ~200 m horizontal extent, is likely a deeper structure. Although our results do not provide the resolution necessary to resolve the relatively shallow small-scale structures associated with the Old Faithful conduit and cavity, these two reservoirs might be structurally related based on their inferred spatial distribution (Figure 4). Additionally, our 0.5–5 Hz Rayleigh wave phase velocity measurements indicate that our study area has two distinct geological units corresponding to the lateral seismic velocity contrast beneath the Old Faithful sinter. This suggests that the location of the deep reservoir is likely controlled by its complexly fractured source volume associated with a rhyolitic lava deposit in the NE acting as a relatively unfractured/consolidated barrier to vertical fluid accent (Figure 4). Although the presence of some hydrothermal features in this unit suggests some fluids are able to

percolate through to the surface, the relativity highly fractured glacial deposits SW of Old Faithful geyser accommodates most of the vertical fluid flow. Higher-resolution imaging of the reservoir was prohibited by the limited station distribution, limited source stations, and the limited time duration (<2 weeks) of our array. Considering the potential time-dependent variability of this hydrothermal feature, future deployments are needed to characterize the temporal variation of this subsurface feature to better constrain its spatial extent.

4. Conclusions

In this study, we investigated the shallow hydrothermal structure of the Yellowstone Upper Geyser Basin including Old Faithful geyser using a temporary seismic deployment recording continuously for 2 weeks. A careful examination and analysis of the spatial distribution of the resulting cross-correlation functions (CCFs) shows a distinct transition from slower phase velocities in the SW to faster velocities in the NE of the Old Faithful area. Moreover, a strong frequency-dependent waveform distortion is observed in the CCFs that transverses the SW area of the Old Faithful study area that we interpret as a highly fractured and porous hydrothermal reservoir with an estimated porosity around 30% occupying the relatively deeper (~10–60 m deep) portion beneath the western part of Old Faithful geyser. The hydrothermal reservoir located SW of the Old Faithful conduit is interpreted to be Old Faithful geyser system and is controlled/limited by the local heterogeneities in structure, variations in fluid flow and gas pressure, etc. Outstanding research questions associated with Old Faithful geyser system include the following: (1) identifying the three-dimensional subsurface structure of the entire Upper Basin Geyser system to reveal the complexity of the deeper hydrothermal system, (2) imaging the uppermost structure (<50 m) which constrains the spatial dimensions of the highly fractured medium that sources the Old Faithful geyser system, and (3) investigating the temporal variability of this subsurface highly fractured feature to better understand the dynamic fluid properties of geyser eruptions, and comeasurements of ground motion with high-precision GPS during seismic observations to evaluate source volume stresses and pore pressures of the entire hydrothermal system.

Acknowledgments

We would like to thank Jacob Lowenstern and Shaul Hurwitz for the thorough reviews; the valuable comments and suggestions have greatly benefited this manuscript. This research is supported by National Science Foundation grant CyberSEES-1442665 and the King Abdullah University of Science and Technology (KAUST) under award OCRF-2014-CRG3-2300. We especially thank the National Park Service, Yellowstone National Park, for permission to conduct this field experiment, YNP permit # YELL-2015-SCI-0114, and for providing collaborative support and field personnel. We also thank FairfieldNodal for sending two engineers to assist us with the deployment. Fieldwork for this project was partially supported by the Brinson Foundation and the Carrico Fund. The noise cross-correlations used in this study can be downloaded from http://noise.earth.utah.edu/UGB_CCF_GRL_2017.tar.

References

Abendini, A. A., Robinson, J. E., Muffler, L. P., White, D. E., Beeson, M. H., & Truesdell, A. H. (2015), Database for the geologic map of upper Geyser Basin, Yellowstone National Park, Wyoming (no. 911). US Geological Survey.

Allen, E. T., & Day, A. L. (1935). *Hot Springs of the Yellowstone National Park* (Vol. 466, p. 525). Washington: Carnegie Inst. Washington Publ.

Bensen, G. D., Ritzwoller, M. H., Barmin, M. P., Levshin, A. L., Lin, F., Moschetti, M. P., … Yang, Y. (2007). Processing seismic ambient noise data to obtain reliable broad-band surface wave dispersion measurements. *Geophysical Journal International*, *169*(3), 1239–1260.

Christiansen, R. L. (2001), The Quaternary and Pliocene Yellowstone plateau volcanic field of Wyoming, Idaho, and Montana, United States Geological Survey. Professional Paper, 729-G (pp. 145).

Christiansen, R. L., J. B. Lowenstern, R. B. Smith, H. Heasler, L. A. Morgan, M. Nathenson, L. G. Mastin, L. J. P. Muffler, and J. E. Robinson (2007), Preliminary assessment of volcanic and hydrothermal hazards in Yellowstone National Park and vicinity, U.S. Geological Survey Open-File Report 2007-071 (pp. 94).

Chu, R., Helmberger, D. V., Sun, D., Jackson, J. M., & Zhu, L. (2010). Mushy magma beneath Yellowstone. *Geophysical Research Letters*, *37*, L01306. https://doi.org/10.1029/2009GL041656

Fenner, C. N. (1936). Borehole investigations in Yellowstone Park. *Journal of Geology*, *44*(2, Part 2), 225–315.

Fournier, R. O. (1969). Old faithful: A physical model. *Science*, *163*(3864), 304–305.

Hurwitz, S., Kumar, A., Taylor, R., & Heasler, H. (2008). Climate-induced variations of geyser periodicity in Yellowstone National Park, USA. *Geology*, *36*(6), 451–454. https://doi.org/10.1130/G24723A.1

Hurwitz, S., & Lowenstern, J. B. (2014). Dynamics of the Yellowstone hydrothermal system. *Reviews of Geophysics*, *52*, 375–411. https://doi.org/10.1002/2014RG000452

Hurwitz, S., & Manga, M. (2017). The fascinating and complex dynamics of geyser eruptions. *Annual Review of Earth and Planetary Sciences*, *45*, 31–59.

Hurwitz, S., Sohn, R. A., Luttrell, K., & Manga, M. (2014). Triggering and modulation of geyser eruptions in Yellowstone National Park by earthquakes, earth tides, and weather. *Journal of Geophysical Research*, *119*, 1718–1737. https://doi.org/10.1002/2013JB010803

Husen, S., Taylor, R., Smith, R. B., & Heasler, H. (2004). Changes in geyser eruption behavior and remotely triggered seismicity in Yellowstone National Park produced by the 2002 *M* 7.9 Denali fault, earthquake, *Alaska*. *Geology*, *32*(6), 537–540. https://doi.org/10.1130/G20381.1

Hutchinson, R. A., Westphal, J. A., & Kieffer, S. W. (1997). *In situ* observations of Old Faithful Geyser. *Geology*, *25*, 875–878.

Karlstrom, L., Hurwitz, S., Sohn, R., Vandemeulebrouck, J., Murphy, F., Rudolph, M. L., … McCleskey, R. B. (2013). Eruptions at Lone Star Geyser, Yellowstone National Park, USA: 1. Energetics and eruption dynamics. *Journal of Geophysical Research*, *118*, 4048–4062. https://doi.org/10.1002/jgrb.50251

Kedar, S., Kanamori, H., & Sturtevant, B. (1998). Bubble collapse as the source of tremor at Old Faithful Geyser. *Journal of Geophysical Research*, *103*, 24,283–24,299. https://doi.org/10.1029/98JB01824

Kedar, S., Sturtevant, B., & Kanamori, H. (1996). The origin of harmonic tremor at Old Faithful Geyser. *Nature*, *379*(6567), 708–711.

Kieffer, S. W. (1984). Seismicity at Old Faithful Geyser: An isolated source of geothermal noise and possible analogue of volcanic seismicity. *Journal of Volcanology and Geothermal Research*, *22*(1–2), 59–95.

Lin, F. C., Li, D., Clayton, R. W., & Hollis, D. (2013). High-resolution 3D shallow crustal structure in Long Beach, California: Application of ambient noise tomography on a dense seismic array. *Geophysics*, *78*(4), Q45–Q56.

Lin, F. C., Moschetti, M. P., & Ritzwoller, M. H. (2008). Surface wave tomography of the western United States from ambient seismic noise: Rayleigh and Love wave phase velocity maps. *Geophysical Journal International*, *173*(1), 281–298.

Lin, F. C., & Ritzwoller, M. H. (2011). Helmholtz surface wave tomography for isotropic and azimuthally anisotropic structure. *Geophysical Journal International*, *186*(3), 1104–1120.

Lin, F. C., Tsai, V. C., & Schmandt, B. (2014). 3-D crustal structure of the western United States: Application of Rayleigh-wave ellipticity extracted from noise cross-correlations. *Geophysical Journal International*, *198*(2), 656–670.

Marler, G. D., & White, D. E. (1975). Seismic geyser and its bearing on the origin and evolution of geysers and hot springs of Yellowstone National Park. *Geological Society of America Bulletin*, *86*(6), 749–759.

Muffler, L. J., White, D. E., Beeson, M. H., & Truesdell, A. H. (1982). Geologic map of Upper Geyser Basin, Yellowstone National Park, Wyoming (No. 1371).

Munoz-Saez, C., Manga, M., Hurwitz, S., Rudolph, M. L., Namiki, A., & Wang, C.-Y. (2015). Dynamics within geyser conduits, and sensitivity to environmental perturbations: Insights from a periodic geyser in the El Tatio geyser field, Atacama Desert, Chile. *Journal of Volcanology and Geothermal Research*, *292*, 41–55. https://doi.org/10.1016/j.jvolgeores.2015.01.002

Rudolph, M., & Sohn, R. A. (2017). A model for internal oscillations in geysers, with application to old faithful (Yellowstone, USA). *Journal of Volcanology and Geothermal Research*, *343*, 17–24. https://doi.org/10.1016/j.jvolgeores.2017.04.023

Smith, R. B., Jordan, M., Steinberger, B., Puskas, C., Farrell, J., Waite, G. P., … O'Connell, R. (2009). Geodynamics of the Yellowstone hotspot and mantle plume: Seismic and GPS imaging, kinematics, and mantle flow. *Journal of Volcanology and Geothermal Research*, *188*(1-3), 26–56.

Smith, R. B., & Siegel, L. (2000). *Windows into the Earth: The geologic story of Yellowstone and Grand Teton National Parks* (p. 242). New York: Oxford University Press.

Snieder, R. (2004), Extracting the Green's function from the correlation of coda waves: A derivation based on stationary phase. *Physical Review E, 69(4)*, 046610.

Vandemeulebrouck, J., Roux, P., & Cros, E. (2013). The plumbing of Old Faithful Geyser revealed by hydrothermal tremor. *Geophysical Research Letters*, *40*, 1989–1993. https://doi.org/10.1002/grl.50422

Waite, G. P., Smith, R. B., & Allen, R. L. (2006). VP and VS structure of the Yellowstone hot spot from teleseismic tomography: Evidence for an upper mantle plume. *Journal of Geophysical Research*, *111*, B04303. https://doi.org/10.1029/2005JB003867

Wang, Y., Lin, F. C., Schmandt, B., & Farrell, J. (2017). Ambient noise tomography across Mount St. Helens using a dense seismic array. *Journal of Geophysical Research: Solid Earth*, *122*, 4492–4508. https://doi.org/10.1002/2016JB013769

White, D. E., Fournier, R. O., Muffler, L. J. P., & Truesdell, A. H. (1975). Physical results of research drilling in thermal areas of Yellowstone National Park, Wyoming, U.S. Geological Survey Professional Paper 892 (pp. 70).